

High-speed computational ghost imaging with compressed sensing based on a convolutional neural network

Hao Zhang

*School of Physics and Physical Engineering,
Qufu Normal University, Qufu 273165, China*

Deyang Duan

*School of Physics and Physical Engineering,
Qufu Normal University, Qufu 273165, China
Shandong Provincial Key Laboratory of Laser Polarization and Information Technology,
Research Institute of Laser, Qufu Normal University, Qufu 273165, China*

Computational ghost imaging (CGI) has recently been intensively studied as an indirect imaging technique. However, the speed of CGI cannot meet the requirements of practical applications. Here, we propose a novel CGI scheme for high-speed imaging. In our scenario, the conventional CGI data processing algorithm is optimized to a new compressed sensing (CS) algorithm based on a convolutional neural network (CNN). CS is used to process the data collected by a conventional CGI device. Then, the processed data are trained by a CNN to reconstruct the image. The experimental results show that our scheme can produce high-quality images with much less sampling than conventional CGI. Moreover, detailed comparisons between the images reconstructed using our approach and with conventional CS and deep learning (DL) show that our scheme outperforms the conventional approach and achieves a faster imaging speed.

I. INTRODUCTION

Ghost imaging is an indirect imaging technique based on quantum properties (e.g., quantum entanglement or intensity correlation) of the light field[1-3]. Compared to conventional optical imaging techniques, ghost imaging requires two light beams: a reference light beam, which never illuminates the object and is directly measured by a detector with a spatial resolution (e.g., a charge-coupled device) and an object light beam, which, after illuminating the object, is measured by a bucket detector with no spatial resolution. By correlating the photocurrents from the two detectors, the ghost image is retrieved. Previous works show that ghost imaging has potential applications in remote sensing[4,5], light detection and ranging (lidar)[6,7], medical imaging[8-10], and super-resolution imaging[11,12]. However, conventional ghost imaging requires two optical paths, which severely limits its application. Fortunately, Shapiro creatively introduced the concept of computational ghost imaging (CGI) in 2008[13]. In the CGI setup, the idle light is obtained by calculation, so the reference light path is omitted in the experimental apparatus[14]. Compared with conventional ghost imaging, CGI is more suitable for application in remote sensing, radar, and other fields.

After more than 10 years, CGI theory and experiments have matured. However, CGI is still in the laboratory stage. One of the critical problems is that the imaging speed cannot meet practical applications. Generally, to produce a clear image, conventional CGI, including conventional ghost imaging, takes approximately 5 minutes, which obviously cannot meet the requirements of practical application, especially those of moving target imaging. How to improve the speed of ghost imaging is one of the key factors for realizing its application. Compressed sensing (CS)[15-18] and deep learning (DL)[19-22] greatly improve the imaging speed, but there is still a gap compared with the speed of classical optical imaging.

In this article, we propose a novel CGI scheme with CS based on a conventional neural network (CS-CNN) to improve the imaging speed. The setup is based on a conventional CGI experimental apparatus. First, the data collected by the CGI device are compressed by the conventional CS algorithm; then, the processed data is trained to reconstruct the ghost image. This scheme combines the advantages of CS with a low sampling rate and a CNN for fast image reconstruction. Theoretical and experimental results show that this scheme is significantly faster than conventional CS and a conventional DL algorithm with a CNN under the condition of obtaining the same quality image.

II. THEORY

We use a conventional CGI experimental device in our work. The setup is shown in Fig. 1. In the setup, a quasi-monochromatic laser illuminates an object $T(\rho)$, and the reflected light carrying the object information is modulated by a spatial light modulator. A bucket detector collects the modulated light $E_{di}(\rho, t)$. Correspondingly, the calculated light $E_{ci}(\rho', t)$ can be obtained by diffraction theory. The object image can be reconstructed by correlating the signal output by the bucket detector and calculated signal[23-25]; i.e.,

$$G(\rho, \rho') = \left\langle |E_{di}(\rho, t)|^2 |E_{ci}(\rho', t)|^2 \right\rangle - \left\langle |E_{di}(\rho, t)|^2 \right\rangle \left\langle |E_{ci}(\rho', t)|^2 \right\rangle \quad (1)$$

where $\langle \cdot \rangle$ stands for an ensemble average. The subscript $i = 1, 2, \dots, n$ denotes the i th measurement, and n denotes the total number of measurements. For simplicity, the object function $T(\rho)$ is contained in $E_{di}(\rho, t)$.

The flow chart of the CS-CNN is shown in Fig. 2. In the following, we briefly introduce the process of this algorithm. The algorithm mainly consists of three parts: (i) a conventional CS program to compress the data collected by the CGI device; (ii) a conventional CGI process program; and (iii) a 10-layer CNN constructed for the training data.

In the conventional CGI device, a set of data (n) are measured by bucket detector. Correspondingly, according to the diffraction theory of light, the distribution of the idle light field in the object plane can be obtained. Thus, we obtain n 200×200 data points. Each data point is divided into 20×20 blocks without overlapping. According to CS theory[? ?], the random Gaussian matrix is used to process the data. The rows of 20×20 data blocks are arranged into a column vector to obtain a 400-dimensional column vector. In this article, the measurement rate is $MR = 0.25$, thus the size of the measurement matrix is 100×400 . Finally, a 100-dimensional measurement vector is obtained. The above process can be expressed as

$$y = \phi x \quad (2)$$

where $\phi \in R^{M \times N}$ ($M \ll N$) is the measurement basis matrix, $x \in R^N$ represents the vectorized image block, and $y \in R^M$ is the measurement vector. N/M represents the measurement rate. Following the above steps, we can further compress the data to 50 dimensions.

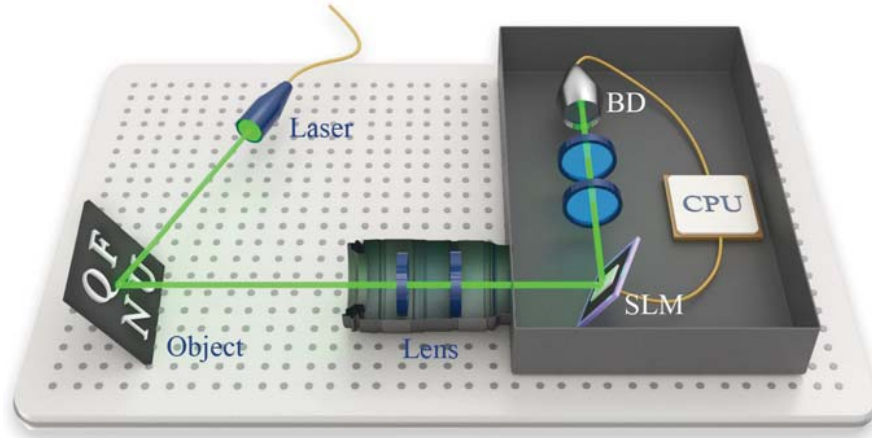


FIG. 1. Setup of the computational ghost imaging system with compressed sensing based on a convolutional neural network. SLM: spatial light modulator, BD: bucket detector.

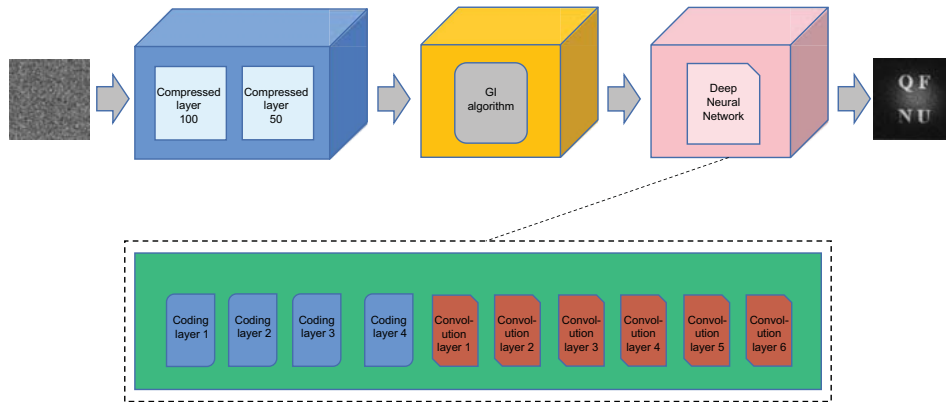


FIG. 2. Network structure of the proposed CS-CNN

A new set of data is obtained by processing the above data with a conventional CGI program. Then, a 10-layer CNN is constructed to train the data. Layers 1-4 of the network are stacked autoencoders, and layers 5-10 are convolution layers. The measurement matrix is replaced by a stacked autoencoder, and the input layer is 20×20 data blocks. All the rows are arranged into a 400×1 column vector. If the number of neurons in the first layer is C , the measurement rate is $MR = C/400$. The first layer of the network is connected to the column vector x converted from the input image block, and the number of neurons C is set according to different measurement rates. The activation function is a rectified linear unit (ReLU) function, which outputs the C -dimensional column vector y ; i.e.,

$$y = T(W_1 x + b_1)$$

where T represents the ReLU activation function and W_1 represents the weight parameter vector of neurons. in the first layer, and b_1 represents the bias of neurons in the first layer.

The second layer of the network is fully connected to the first layer, which has 400 neurons. Take the output y of the first layer as the input, output x , and the activation function is the ReLU function. In the same way, the third layer is fully connected to the second layer, with 100 neurons. The fourth layer is fully connected to the third layer, with 400 neurons. The initial reconstructed image block vector is rearranged into 20×20 image blocks according to the original row and column to obtain the preliminary reconstructed image block.

Finally, the CNN is used to reconstruct the image block accurately. The output data of the fourth layer are taken as the input of the fifth layer. In the fifth layer, 64 11×11 convolution kernels are used to generate 64 10×10 feature maps. The sixth layer of the network is connected to the fifth layer (a convolution layer), and 32 1×1 convolution kernels are used to generate 32 20×20 characteristic graphs. The seventh layer of the network is connected to the

sixth layer (a convolution layer), and a 7×7 convolution kernel is used to generate a 20×20 feature map. The eighth layer of the network is connected to the seventh layer (a convolution layer), and 64 11×11 convolution cores are used to generate 64 20×20 feature maps. The ninth layer of the network is connected to the eighth layer (a convolution layer), and 32 1×1 convolution kernels are used to generate 32 20×20 characteristic graphs. The activation function of the above process is a ReLU function. The tenth layer of the network is connected to the ninth layer (a convolution layer). A 7×7 convolution kernel is used. The number of zeros in the tenth layer (a convolution layer) is 3, and the output of the activation function is not used to generate the reconstructed image block of size 20×20 .

In the deep learning framework Caffe, the 10-layer network is trained in an unsupervised way, and the loss function is

$$L(\{W\}) = \frac{1}{T} \sum_1^T \|F(x_i, \{W\}) - x_i\|^2$$

where fan_{in} represents the number of input units in the i th layer and fan_{out} represents the number of output neurons in the i th layer; the number of input neurons in the first layer is 0, and the number of output neurons in the fourth layer is 0. In the 5th to 10th layers of the network, the initial weight distribution is subject to a Gaussian distribution with a mean of 0 and a variance of 0.01. In layers 1-10 of the network, the initial offset values are set to 0. After the deep neural network, the reconstructed image blocks are obtained, and then the image blocks are rearranged according to the original row, and the row values are rearranged according to the index.

III. EXPERIMENTS AND RESULTS

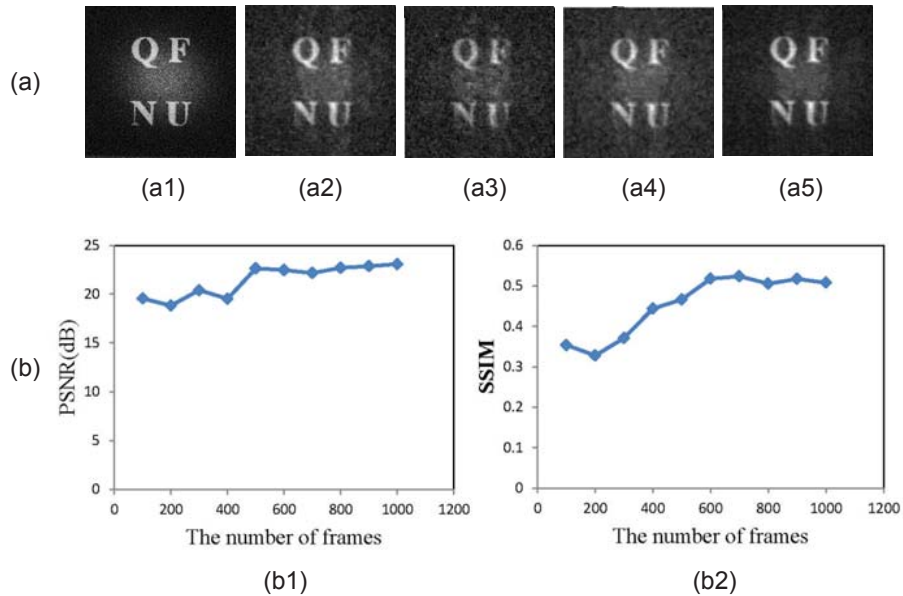


FIG. 3. The ghost image reconstructed by computational ghost imaging with compressed sensing based on a convolutional neural network. (a1) Classical image. The number of frames in the reconstructed ghost images are (a2) 100, (a3) 200, (a4) 300, (a5) 400. (b) The PSNR and SSIM curves of reconstructed image with different frames number.

The experimental setup is schematically shown in Fig. 1. A standard monochromatic laser (30 mW, Changchun New Industries Optoelectronics Technology Co., Ltd. MGL-III-532) with wavelength $\lambda = 532 \text{ nm}$ illuminates an object (Qufu Normal University, QFNU). The light reflected by the object focus on a two-dimensional amplitude-only ferroelectric liquid crystal spatial light modulator (Meadowlark Optics A512-450-850) with 512×512 addressable $15 \mu\text{m} \times 15 \mu\text{m}$ pixels through the lens. A bucket detector collects the modulated light. Correspondingly, the reference signal is obtained by MATLAB software. The ghost image is reconstructed by the CS-CNN. In this experiment, the sampling rate is $MR = 0.25$ and the number of training sets is 1000.

Fig. 3 shows a set of experimental results. Fig. 3(a1) is the object. Figs. 3(a2 - a5) represent reconstructed ghost images with different numbers of frames. The results show that the image quality is significantly improved by

increasing the number of frames. High-quality ghost images comparable to classical optical imaging can be produced with little data. To quantitatively analyze the quality of the reconstructed image at different frames, peak signal to noise ratio (PSNR) and structural similarity index (SSIM) are used as our evaluation index. As can be seen from Fig. 3(b), despite the number of samples is very small, the reconstructions are still in reasonable quality.

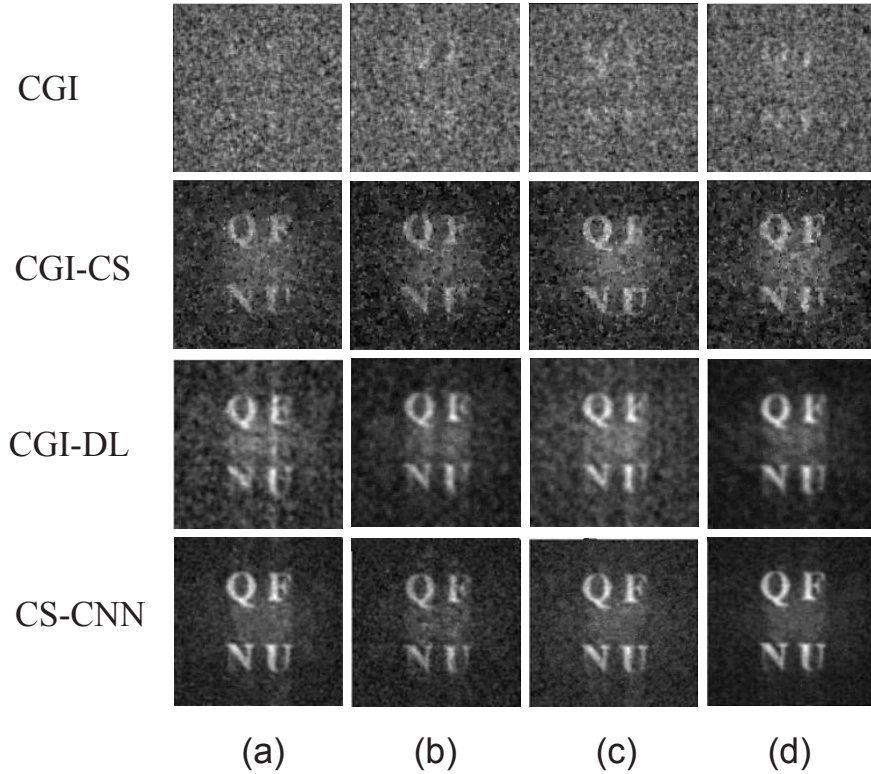


FIG. 4. Detailed comparisons between the ghost image reconstructed using the computational ghost imaging (CGI) algorithm, conventional compressed sensing (CS) algorithm, deep learning (DL) algorithm and compressed sensing algorithm based on a convolutional neural network (CS-CNN). The number of frames is (a) 100, (b) 200, (c) 200, and (d) 400.

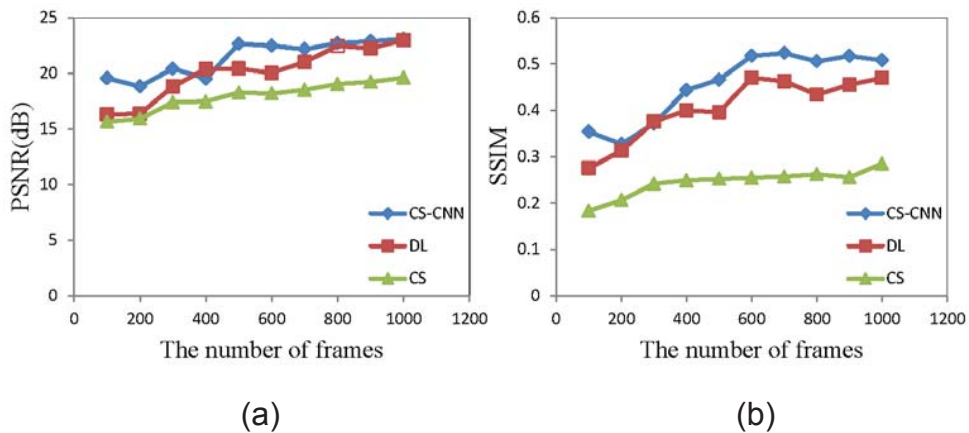


FIG. 5. The PSNR and SSIM curves of reconstructed images of CS, DL and CS-CNN with different frames number, respectively.

We compare the conventional, CS, DL, and CS-CNN CGI algorithms based on the same experimental data. The conventional CS algorithm and CS-CNN algorithm have the same sampling rate; i.e., $MR = 0.25$. The DL algorithm and CS-CNN algorithm set the same dataset. i.e., 1000. Fig. 4 shows that the frame number of the CS-CNN algorithm

is obviously less than that of other algorithms to produce ghost images with the same quality. The quantitative results (Fig.5) show that the PSNR of CGI with CS-CNN is average 7% higher than that of CGI with DL under the same reconstructed frame number, SSIM increased by 12% on average[26]. Consequently, under the condition of producing the same image quality, CS-CNN has the faster imaging speed.

IV. CONCLUSIONS

We have proposed a novel method for high-speed CGI. This method combines the advantages of the CS algorithm and CNN algorithm. We analyzed the performance of the conventional CGI, CS, and DL algorithms under the same conditions and observed that our CS-CNN scheme outperforms the other methods, especially when the sampling number is very small. To our knowledge, CS based on a CNN is the fastest CGI method to date. This method significantly reduces the data acquisition time in CGI, providing a promising solution to these challenges that prohibits the use of CGI in practical applications.

V. FUNDING

This project was supported by the National Natural Science Foundation (China) under grant nos. 11704221, 11574178 and 61675115 and the Taishan Scholar Project of Shandong Province (China) under grant no. tsqn201812059.

VI. DISCLOSURES

The authors declare that there are no conflicts of interest related to this article.

-
- [1] T. B. Pittman, Y. H. Shih, D. V. Strekalov, and A. V. Sergienko. Optical imaging by means of two-photon quantum entanglement. *Phys. Rev. A* 52, R3429 (1995).
 - [2] J. Cheng and S.-S. Han. Incoherent coincidence imaging and its applicability in X-ray diffraction. *Phys. Rev. Lett.* 92, 093903 (2004).
 - [3] X. H. Chen, Q. Liu, K. H. Luo, and L. A. Wu. Lensless ghost imaging with true thermal light. *Opt. Lett.* 34, 695-697 (2009).
 - [4] B. I. Erkmen. Computational ghost imaging for remote sensing. *J. Opt. Soc. A* 29, 782-789 (2012).
 - [5] D. Y. Duan, Z. X. Man, and Y. J. Xia. Nondegenerate wavelength computational ghost imaging with thermal light. *Opt. Express* 27, 25187-25195 (2019).
 - [6] C. Q. Zhao, W. L. Gong, M. L. Chen, E. R. Li, H. Wang, W. D. Xu, and S. S. Han. Ghost imaging lidar via sparsity constraints. *Appl. Phys. Lett.* 101, 141123 (2012).
 - [7] W. L. Gong, C. Q. Zhao, H. Yu, M. L. Chen, W. D. Xu, and S. S. Han. Three-dimensional ghost imaging lidar via sparsity constraint. *Sci. Rep.* 6, 26133 (2016).
 - [8] D. Pelliccia, A. Rack, M. Scheel, V. Cantelli, and D. M. Paganin. Experimental X-Ray Ghost Imaging. *Phys. Rev. Lett.* 117, 113902 (2016).
 - [9] H. Yu, R. Lu, S. Han, H. Xie, G. Du, T. Xiao, and D. Zhu. Fourier-Transform Ghost Imaging with Hard X Rays. *Phys. Rev. Lett.* 117, 113901 (2016).
 - [10] A. Zhang, Y. He, L. Wu, L. Chen and B. Wang. Tabletop x-ray ghost imaging with ultra-low radiation. *Optica* 5, 374-377 (2018).
 - [11] W. Li, Z. Tong, K. Xiao, Z. Liu, Q. Gao, J. Sun, S. Liu, S. Han, and Z. Wang. Single-frame wide-field nanoscopy based on ghost imaging via sparsity constraints. *Optica* 6, 1515-1523 (2019).
 - [12] W. Gong and S. Han. High-resolution far-field ghost imaging via sparsity constraint. *Sci. Rep.* 5, 9280 (2015).
 - [13] J. H. Shapiro. Computational ghost imaging. *Phys. Rev. A* 78, 061802(R) (2008).
 - [14] Y. Bromberg, O. Katz, and Y. Silberberg. Ghost imaging with a single detector. *Phys. Rev. A* 79, 053840 (2009).
 - [15] O. Katza, Y. Bromberg, and Y. Silberberg. Compressive ghost imaging. *Appl. Phys. Lett.* 95, 131110 (2009).
 - [16] V. Katkovnik and J. Astola. Compressive sensing computational ghost imaging. *J. Opt. Soc. Am. A* 29, 1556-1567 (2012).
 - [17] W. K. Yu, M. F. Li, X. R. Yao, X. F. Liu, L. A. Wu, and G. J. Zhai. Compressive sensing computational ghost imaging. *Opt. Express* 22, 7133-7144 (2014).
 - [18] Z. Chen, J. Shi, and G. Zeng. Object authentication based on compressive ghost imaging. *Appl. Opt.* 55, 8644-8650 (2016).
 - [19] M. Lyu, W. Wang, H. Wang, W. Wang, G. Li, N. Chen, and G. Situ. Deep-learning-based ghost imaging. *Sci. Rep.* 7, 17865 (2017).

- [20] Y. He, G. Wang, G. Dong, S. Zhu, H. Chen, A. Zhang, and Z. Xu. Ghost imaging based on deep learning . *Sci. Rep.* 8, 6469 (2018).
- [21] T. Shimobaba, Y. Endo, T. Nishitsuji, T. Takahashi, Y. Nagahama, T. Hasegawa, M. Sano, R. Hirayama, T. Kakue, A. Shiraki, and T. Ito . Computational ghost imaging using deep learning . *Opt. Commun.* 413, 147-151 (2018).
- [22] G. Barbastathis, A. Ozcan, and G. Situ . On the use of deep learning for computational imaging . *Optica* 6, 921-943 (2019).
- [23] X. L. Yin, Y. J. Xia, and D. Y. Duan. On the use of deep learning for computational imaging . *Opt. Express* 26, 18944-18949 (2018).
- [24] W.-J. Jiang, X.-Y. Li, X.-L. Peng, and B.-Q. Sun. Imaging high-speed moving targets with a single-pixel detector . *Opt. Express* 28, 7889-7897 (2020).
- [25] D.-F. Shi, C.-Y. Fan, P.-F. Zhang, H. Shen, J.-H. Zhang, C.-H. Qiao, and Y.-J. Wang. Two-wavelength ghost imaging through atmospheric turbulence. *Opt. Express* 21, 2050-2064 (2013).
- [26] Y.-H. Liu, S.-Y. Liu, and F.-X. Fu. Optimization of Compressed Sensing Reconstruction Algorithms Based on Convolutional Neural Network. *Comput. Sci.* 47, 143-148 (2020).